Gerringer ME, Linley TD, Jamieson AJ, Goetze E, Drazen JC.
Pseudoliparis swirei sp. nov.: A newly-discovered hadal snailfish (Scorpaeniformes: Liparidae) from the Mariana Trench.
***Zootaxa* 2017, 4358(1), 161-177**

Zootaxa 4358 (1): 161–177
http://www.mapress.com/j/zt/

Article

ISSN 1175-5326 (print edition)
ZOOTAXA
ISSN 1175-5334 (online edition)

https://doi.org/10.11646/zootaxa.4358.1.7
http://zoobank.org/urn:lsid:zoobank.org:pub:84494502-9E85-49DA-8530-092AF8918D88

Pseudoliparis swirei sp. nov.: A newly-discovered hadal snailfish (Scorpaeniformes: Liparidae) from the Mariana Trench

MACKENZIE E. GERRINGER[1], THOMAS D. LINLEY[2], ALAN J. JAMIESON[2], ERICA GOETZE[1] & JEFFREY C. DRAZEN[1]

[1]*Dept. Of Oceanography, University of Hawai'i at Mānoa, HI 96822.*
E-mail: mgerring@hawaii.edu, jdrazen@hawaii.edu, egoetze@hawaii.edu
[2]*School of Marine Science and Technology, Ridley Building, Newcastle University, Newcastle Upon Tyne, UK. NE1 7RU.*
E-mail: thomas.linley@newcastle.ac.uk, alan.jamieson@newcastle.ac.uk

Abstract

Pseudoliparis swirei **sp. nov.** is described from 37 individuals collected in the Mariana Trench at depths 6898–7966 m. The collection of this new species is the deepest benthic capture of a vertebrate with corroborated depth data. Here, we describe *P. swirei* **sp. nov.** and discuss aspects of its morphology, biology, distribution, and phylogenetic relationships to other hadal liparids based on analysis of three mitochondrial genes. *Pseudoliparis swirei* **sp. nov.** is almost certainly endemic to the Mariana Trench, as other hadal liparids appear isolated to a single trench/ trench system in the Kermadec, Macquarie, South Sandwich, South Orkney, Peru-Chile, Kurile-Kamchatka and Japan trenches. The discovery of another hadal liparid species, apparently abundant at depths where other fish species are few and only found in low numbers, provides further evidence for the dominance of this family among the hadal fish fauna.

Key words: snailfish, *Notoliparis*, description, taxonomy, phylogenetics

Introduction

The Liparidae (snailfishes, Scorpaeniformes), are probably the most geographically and bathymetrically widespread family of marine fishes, including more than four hundred species in about 30 genera with representatives in all oceans where water temperature is temperate to cold. The snailfishes have the widest depth range of any marine fish family (Chernova *et al.* 2004), with habitats ranging from the intertidal to depths exceeding 8,000 m (Linley *et al.* 2016). To date, different, likely endemic, liparid species have been found in seven trenches and troughs, including the Kermadec, Macquarie, South Orkney, South Sandwich, Peru-Chile, Japan, and Kurile-Kamchatka trenches with another species likely in the Puerto Rico Trench (Fujii *et al.* 2010; Pérês 1965). Recent advances in hadal sampling technology have allowed the observation and recovery of these animals and show them to be abundant in those trenches that have been systematically studied (Jamieson *et al*. 2009; Fujii *et al*. 2010; Linley *et al*. 2016). They are a notably successful hadal fish family, extending deeper and/or reaching higher densities than other hadal fishes (Linley *et al.* 2017).

During cruises of the *R/V Falkor* from 9 November to 10 December 2014 and the *R/V Shinyo-maru* from 20 January to 3 February 2017, baited traps collected 37 individuals of a new species of snailfish at depths from 6,898 to 7,966 m in the Mariana Trench. These specimens are probably the deepest collected fish from the ocean bottom with corroborating depth data (see notes on spurious records in Fujii *et al.* 2010), although another remarkable liparid species was filmed (but not recovered) on the same cruise at an even greater depth of 8,143 m (Linley *et al.* 2016). In this paper, we describe and name the new species that was collected and present aspects of its biology.

Accepted by E. Hilton: 24 Oct. 2017; published: 28 Nov. 2017

Materials and methods

Specimens were collected using two free-falling traps (Linley *et al.* 2016) with steel ballast ejected by acoustic release (IXSEA, France; Teledyne Benthos, USA) for retrieval. The holotype and most paratypes were collected in 2014, with one additional paratype collected on 29 Jan 2017 using the same methodology. Traps consisted of an aluminum or fiber glass frame lined with stiff plastic mesh covered with fine mesh netting to minimize specimen damage, attached to a mooring line with glass floatation spheres in 43 cm protective housings (Nautilus Marine Services, Germany) to provide buoyancy. Each trap was baited with mackerel in a nylon mesh bag, and included PVC funnel traps for amphipod collection. Collection sites are shown in Figure 1 and site details are provided in Table 1.

TABLE 1. Collection information. Specimens collected on cruise FK141109 of the *RV Falkor* and SY1615 of the *RV Shinyo-maru*. Number of individual fish collected in each trap deployment (*n*) shown.

Deployment	Date	Latitude	Longitude	Depth (m)	n
TR05	15 Nov 2014	12.59786°N	144.77854°E	7062	1
TR06	16 Nov 2014	12.63390°N	144.75080°E	6914	1
TR07	18 Nov 2014	12.42347°N	144.87058°E	7497	8
TR08	19 Nov 2014	12.42556°N	144.91171°E	7509	4
TR09	21 Nov 2014	12.30274°N	144.67388°E	7929	1
TR10	23 Nov 2014	11.91280°N	144.94450°E	7841	3
TR12	25 Nov 2014	11.81070°N	144.99450°E	6898	1
TR13	26 Nov 2014	11.82600°N	145.00880°E	6974	3
TR19	6 Dec 2014	12.27660°N	144.62020°E	7626	2
TR20	7 Dec 2014	12.34950°N	144.68130°E	7652	4
WT03	16 Nov 2014	12.61026°N	144.76839°E	6961	3
WT04	18 Nov 2014	12.41505°N	144.91187°E	7495	1
WT06	21 Nov 2014	12.30370°N	144.68038°E	7949	1
WT07	23 Nov 2014	11.92730°N	144.96200°E	7907	1
WT08	24 Nov 2014	11.92970°N	144.92880°E	7966	1
WT09	25 Nov 2014	11.81470°N	144.98580°E	6949	2
FT02	29 Jan 2017	11.54290°N	142.18485°E	7581	1

Fin clips and tissue samples for genetic study were preserved in 95% EtOH. Additional tissue samples were frozen at -80ºC for physiological studies. Individuals were fixed in 10% buffered formalin at sea and transferred after five months in stages to 75% EtOH. The specimens have been deposited at the Museum Support Center, the Smithsonian Institution National Museum of Natural History, Suitland, MD, USA (USNM), the Scripps Institution of Oceanography, Marine Vertebrate Collection, La Jolla, CA, USA (SIO), and the Tokyo University of Marine Science and Technology, Museum of Marine Science, Tokyo, Japan (TUMSAT, Supplementary Table 1).

Definitions of counts, measurements, and characters follow Stein *et al*. (2001), Andriashev (2003), and Stein (2012). Museum abbreviations follow Sabaj Perez (2014). Counts of vertebrae, dorsal, and anal fin rays and pre-dorsal fin lengths were obtained from radiographs of specimens. Pectoral and caudal fin ray counts were made by direct examination. Pectoral girdles were removed from four specimens and stained using alizarin red S (Taylor 1967a; b) and alcian blue. Whole specimens were temporarily stained with cyanine blue when necessary (Saruwatari *et al.* 1997).

Selected measurements were made immediately upon retrieval, including total length, standard length, pre-anal fin length, head length, eye width, snout width, and weight. Fresh and preserved measurements of the same characters in each fish were compared to estimate shrinkage caused by preservative osmolarity changes (e.g. Hay 1982; Kristoffersen & Salvanes 1998). Standard lengths (SL) in the Material Examined section are presented as preserved/fresh* mm.

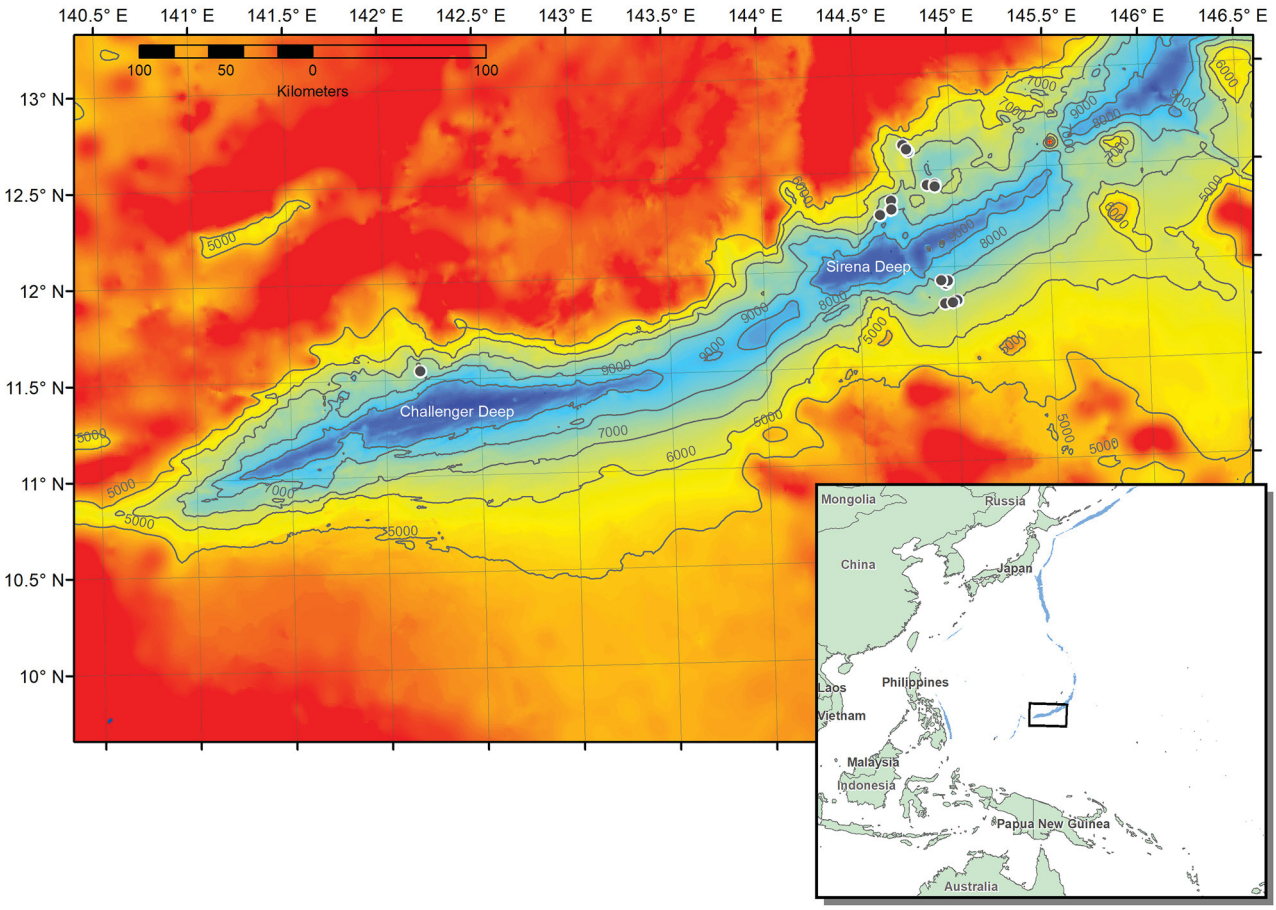

FIGURE 1. Map of collection locations within the Mariana Trench. Bathymetry courtesy of JAMSTEC. Isobaths are added between 5,000 and 9,000 m at 1,000 m intervals.

Counts are given as the median, followed by the range in parentheses. Ratios for proportions are given as percent standard length (%SL) and percent head length (%HL) for the mean first, followed in parentheses by the range for all specimens. For characters that were damaged during preservation, fresh ratios are presented. Ratios taken from fresh measurements are indicated with an asterisk. Ratios taken from photographs of freshly caught specimens are indicated with two asterisks. All ratios are based on comparisons of like measurements, e.g. fresh head length to fresh standard length or preserved vs preserved. Data analysis was conducted using the program R (R Core Development Team 2015) and figures were constructed using the package ggplot2 (Wickam 2009). Ontogenetic trends were investigated through fitted linear models and ANOVA (type-I sum of squares). Imprecision of very small orbit width measurements, leading to heteroscedasticity, was corrected through cubed weighted least squares relative to SL. Results were considered significant at an α of 0.05.

Sex was determined macroscopically. Eggs were removed from mature and maturing females. For the four females with sufficiently ripe eggs, all eggs were counted and those above 1 mm diameter were measured. For the remaining females with distinguishable eggs, maximum egg size was recorded.

DNA was extracted from epaxial muscle tissue from five individuals of *Pseudoliparis swirei* **sp. nov.** and five hadal liparids from the Kermadec Trench (three *Notoliparis kermadecensis* (Nielsen, 1964) and two *Notoliparis stewarti* (Stein, 2016); collection described by Linley *et al.* 2016) with the DNeasy Blood and Tissue Kit (Qiagen), following the manufacturer's protocols. Three mitochondrial gene fragments, 16S rRNA (16S, 1472 bp), cytochrome *b* (Cyt-*b*, 1007 bp) and cytochrome *c* oxidase subunit I (COI, 1399 bp) were amplified in polymerase chain reaction (PCR). PCR cycling included 35 cycles of denaturation at 95ºC for 30 seconds, annealing at 48ºC (16S) or 52ºC (Cyt-*b*, COI) for 30 seconds, and extension at 72ºC for 1 minute. Primers used included 16S_liparids_F (5'-CTA TTA ATA CCC CCA AAT ACC CC-3'), 16S_liparids_R (5'-CGA TGT TTT TGG TAA ACA GGC G-3'), and 16S_liparids_R2 (5'-GAT TTC ATC AGG TAG GGG GAG GGC-3') for 16S rRNA. For Cyt-*b*, primers were Cytb_liparids_F (5'-ATG GCA AGC CTA CGA AAA ACC CAC C-3'), Cytb_liparids_R (5'-

TAT TCT CTA TGA AGC CGG TAA GGG-3'), and Cytb_liparids_R2 (5'-GGG TTA GTT GAG CCT GTT TCG TG-3'). COI primers were COI_liparids_F (5'GCC ATC CTA CCT GTG GCC ATC ACA CG-3'), COI_liparids_R (5'-AGT GGG ATA AAA CAA ATG CGG G-3'), as well as modified versions of the COI primers reported by Ward *et al.* (2005), Liparid_WardsF1 (5'-TCG ACT AAT CAC AAA GAC ATT GGC AC-3'), and Liparid_WardsR1 (5'-TAA ACT TCG GGA TGG CCA AAG AAT CA-3'). PCR products were purified using ExoSAP-IT *Express* (affymetrix, Thermo Fisher Scientific) and Sanger sequencing was performed on an ABI 3730XL with BigDye chemistry. Two sequencing primers were used in addition to PCR primers: 16S_liparids_I (5'-CCA AAA ACA TCG CCT CTT GTA CCC-3') for 16S and COI_liparids_I (5'-CTG ATT CTT TGG CCA TCC CGA AG-3') for COI.

Base calls were confirmed by aligning both strands in Geneious v7.1.8 (Kearse *et al.* 2012), with final alignments for each gene fragment generated by Multiple Sequence Comparison by Log-Expectation (MUSCLE; Edgar 2004; McWilliam *et al.* 2013). The best fit nucleotide substitution model for each alignment was evaluated by Bayesian Information Criterion (BIC), as implemented in jModelTest (Darriba *et al*., 2012; Guindon & Gascuel 2003). The best models were found to be HKY+G for COI and Cyt-*b* and TPM2uf+G for 16S. Average pairwise genetic distances among species were calculated in MEGA6 (Tamura *et al.* 2013), using the closest available model, the Tamura-Nei model with gamma-distributed rate variation (a = 0.1813 [16S], 0.1889 [COI], 0.2314 [Cyt-*b*], model-averaged estimates). Because we included NCBI sequences of liparids *Careproctus rastrinus* (Gilbert & Burke 1912; GenBank Accession JF952697.1, Zhang & Hanner 2011; AB565517.1, AB565629.1, Kai *et al*. 2011), *C. colleti* (Gilbert, 1896; AB565515.1, Kai *et al*. 2011), we trimmed our alignment to include only regions present for all species for genetic distance calculations (COI: 644-bp, Cyt-*b*: 744-bp, 16S: 699-bp).

Phylogenetic trees were inferred under maximum likelihood (ML) using Randomized Axelerated Maximum Likelihood (RAxML, GTRGAMMA model), with node support assessed by 1,000 bootstrap iterations (Stamatakis 2014). Bayesian phylogenetic inference was conducted in MrBayes 3.2, using the GTR+gamma nucleotide substitution model. Markov Chain Monte Carlo (MCMC) sampling of the posterior distribution was conducted for 1 million generations, with sampling every 500 generations. Sequences from *Pseudoliparis belyaevi* (Andriashev & Pitruk, 1993) from the Japan Trench (T.P. Satoh, unpublished data, NMST 92445, 92446, 92447) were included in our alignments to assess placement of this new Mariana species into genus. The smooth lumpfish, *Aptocyclus ventricosus* (Pallas, 1769; GenBank Accession NC_008129.1; Miya *et al*., 2003), was chosen as an outgroup as the most closely related species with full gene sequences available for 16S rRNA, mtCOI, and Cyt-*b*. To evaluate the influence of outgroup taxon on tree topology, additional analyses were conducted with the more closely related genus *Careproctus* as an outgroup, using a shorter alignments due to limited outgroup data (16S: 696-bp *C. rastrinus* GenBank Accession AB565650.1, *C. colletti* AB565627.1; COI: 645-bp *C. cypselurus* GU440261.1, *C. rastrinus* JF952697; Cyt-*b*: 744-bp *C. rastrinus* ASB565625.1, *C. phasma* (Gilbert, 1896) LC036287.1) with all analysis steps as described above. The Interactive Tree of Life (iTOL v3; Letunic & Bork 2007) was used for visualization of trees.

Pseudoliparis swirei **Gerringer & Linley sp. nov.**

Figures 2, 3, 4, 5; Tables 2, 3

Mariana snailfish: Linley *et al.* 2016 (page 105, Figure 4a)
Mariana snailfish: Linley *et al*. 2017 (page 42, Figure 6.43)
Mariana snailfish/Mariana liparid: Gerringer *et al.* 2017a (page 111)
Mariana liparid/Liparidae sp. nov: Gerringer *et al.* 2017b (page 137)

Diagnosis. Andriashev and Pitruk (1993) define the genus *Pseudoliparis* as having a well-developed disk and one pair of nostrils and lacking pseudobranchia and pleural ribs, with four radials in the pectoral girdle, which has neither notches nor fenestrae. In this genus, the hypural plate is divided by a distal slit (Andriashev and Pitruk, 1993). Like the other in this genus, *Pseudoliparis swirei* **sp. nov.** (Figures 2, 3) displays these characters, including a moderately well-developed disk, although this is easily damaged in collection. *Pseudoliparis swirei* **sp. nov.** can be distinguished from the two other known *Pseudoliparis* species with the following characters. *Pseudoliparis swirei* **sp. nov.** differs from *P. belyaevi* in the presence of a distinct lower pectoral-fin lobe, similar to that seen in *P. amblystomopsis* (Andriashev, 1955). *Pseudoliparis swirei* has more dorsal-fin rays 55 (51–58) than *P.*

amblystomopsis 49 (49–52), more anal-fin rays 48 (43–49) compared to 43 (42–45), and more vertebrae 61 (56–62), compared to 55–57, although these ranges somewhat overlap. Head length is shorter in *P. swirei* **sp. nov.** (17.0–21.7 %SL) than *P. amblystomopsis* (21.6–24.0 %SL). Comparisons were made according to ranges presented by Andriashev & Pitruk (1993). *Pseudoliparis belyaevi* is known only from the Japan Trench, *P. amblystomopsis* from the Japan and Kurile-Kamchatka trenches, *P. swirei* only from the Mariana Trench.

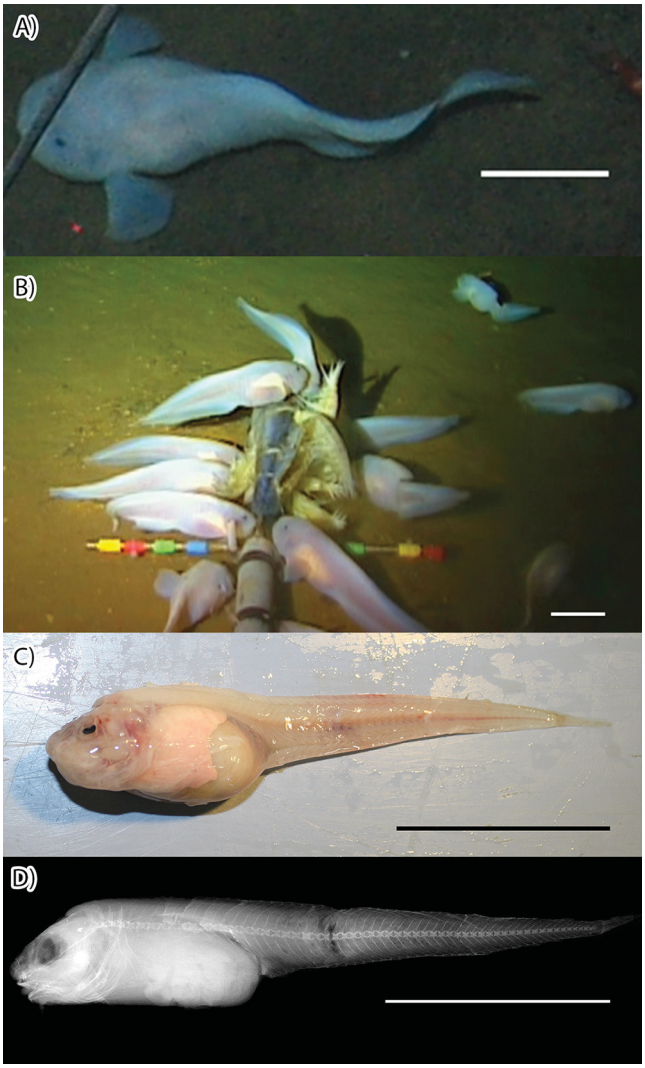

FIGURE 2. A) *In situ* photograph of *Pseudoliparis swirei* **sp. nov.** at 6,198 m. B) a group at 7,485 m. C) Deck photograph of SIO 16-82/HADES 200049. D) Radiograph of SIO 16-86/HADES 200141. Image by Sandra Raredon. Scale indicator 5 cm.

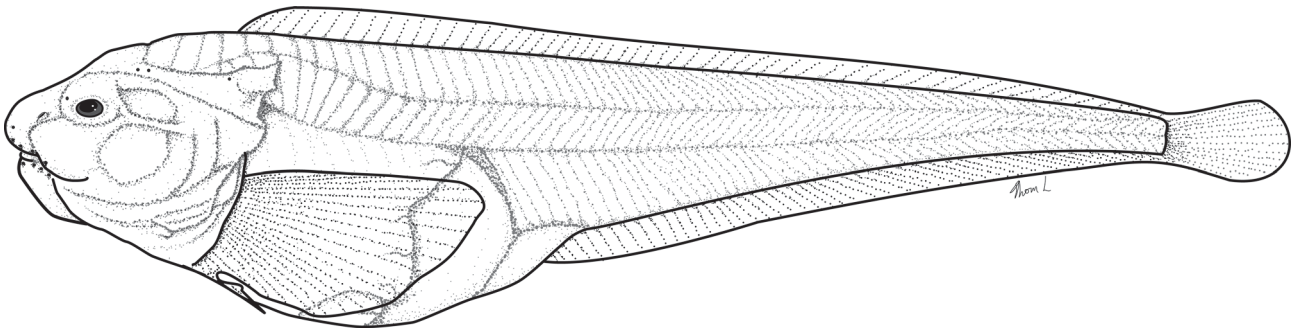

FIGURE 3. Lateral view of *Pseudoliparis swirei* **sp. nov.**. Combined representation of holotype, paratypes, and freshly captured images of paratype USNM 438985/HADES 200133, juvenile, 151 mm. Drawings by Thomas D. Linley.

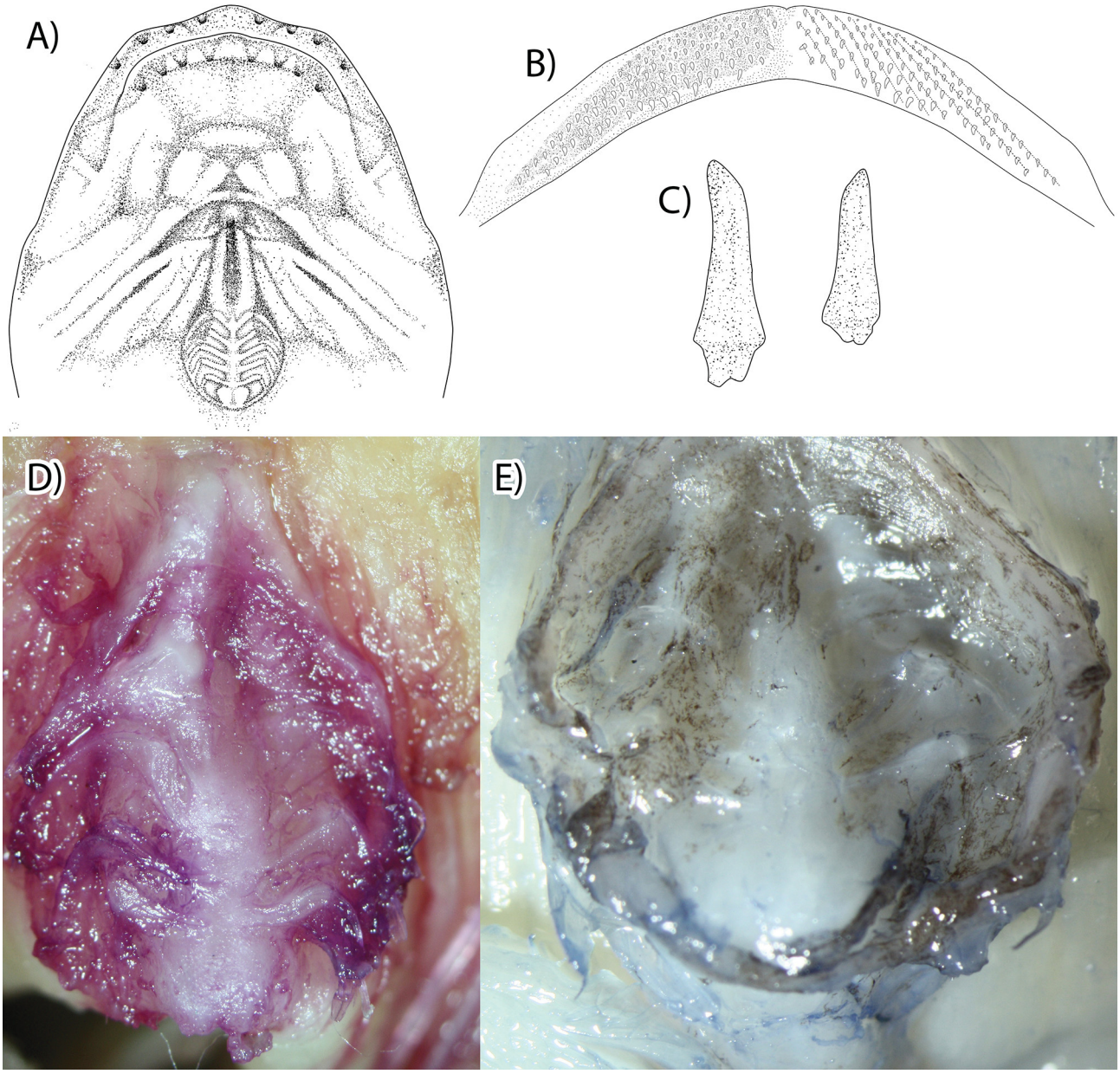

FIGURE 4. A) Ventral view drawing. B) Tooth pattern on maxillary jaw. Counted rows denoted on right side of image. C) Tooth structure of specimen USNM 438996/HADES 200024. D) Disk details of SIO 16-87/HADES 200025 stained with Alizarin Red S. E) Disk of USNM 438995/HADES 200085 stained with Cyanine Blue.

Description. Vertebrae 61 (56–62), dorsal-fin rays 55 (51–58), anal-fin rays 48 (43–49), caudal-fin rays 13 (11–14), pectoral-fin rays 30 (28–32), pectoral radials 4, pyloric caeca 7 (5–9). Ranges of measurements and counts are presented in Table 2. Ratios are presented in Table 3. All individual measurements and counts are available in Supplementary Table 1. Micro-CT scans and a 3D rotatable model of the holotype are available in the Supplementary Material.

Head small, low, and wide, lateral profile anteriorly rounded and rising slowly to occiput, where the angle increases. Head depth about equal to body depth or lower, depending on abdominal fullness. Snout blunt, nostrils single, nares on horizontal with center of eye. Mouth broad, horizontal, subterminal, moderately large; upper jaw reaching to below middle of orbit, oral cleft reaching to below anterior edge of orbit. Teeth simple, sharp canines, innermost largest, arranged in approximately 9 (6–11 maxilla, 7–13 mandible) oblique, irregular rows of up to 20 (6–17 maxilla, 8–20 mandible) teeth each, forming a moderately wide band (2–4 teeth wide) in each jaw (Figure 4). Larger individuals had more teeth per row and more rows of teeth. Maxilla with prominent symphyseal gap, slight gap present in mandible. Pharyngeal teeth well developed, long, sharp, strongly fixed on globular tooth plates. Eye

very small, about 10% head length. Orbit large, its dorsal margin well below that of head. Gill opening small, located completely above pectoral fin, width 5% SL. Opercular flap fleshy, broadly triangular, opercle terminates in two small spines below the flesh. Cephalic pores small, easily damaged; few remaining. Eight widely separated infraorbital and mandibular pores, lacking raised rims. In fresh specimens, the infraorbital and mandibular pores appear sunken and anteriorly orientated within the gelatinous tissue of the head (Figure 4).

Pectoral fin divided into lobes by a moderately deep notch, rudimentary rays absent. Notch rays 5 (3–6), clearly more widely spaced than those of upper and lower lobes, more so in larger individuals. Upper and lower lobe rays closely spaced. Dorsal-most pectoral-fin ray on horizontal between level of upper jaw and lower margin of orbit. Symphysis of pectoral fins and anteriormost ray below rear of orbit. Upper lobe about 15.2% SL (12.6–19.8), lower about 7.8% SL (6.3–12.1). Upper lobe almost extending to anal-fin origin, lower lobe distinct, reaching well behind disk to below middle of upper lobe base. Pectoral radials four, fenestra absent; of four specimens examined (USNM 438996/HADES 200024, USNM 438994/HADES 200027, USNM 438997/HADES 200033, USNM 438989/HADES 200096); one (USNM 438996HADES 200024) had (1+1+1+1), and three (USNM 438994/HADES 200027, USNM 438997/HADES 200033, USNM 438989/HADES 200096) had (3+1) radials, generally round, notches and foramina absent (Figure 5). Radials gradually and irregularly decreasing in size from R1 (largest) to R4 (smallest). Distal radials present under the base of all rays, with the exception of the two most ventral rays (Supplementary Figure 1). Scapula double-headed, posterior head larger and broader than anterior head, coracoid with broad head and long slender helve.

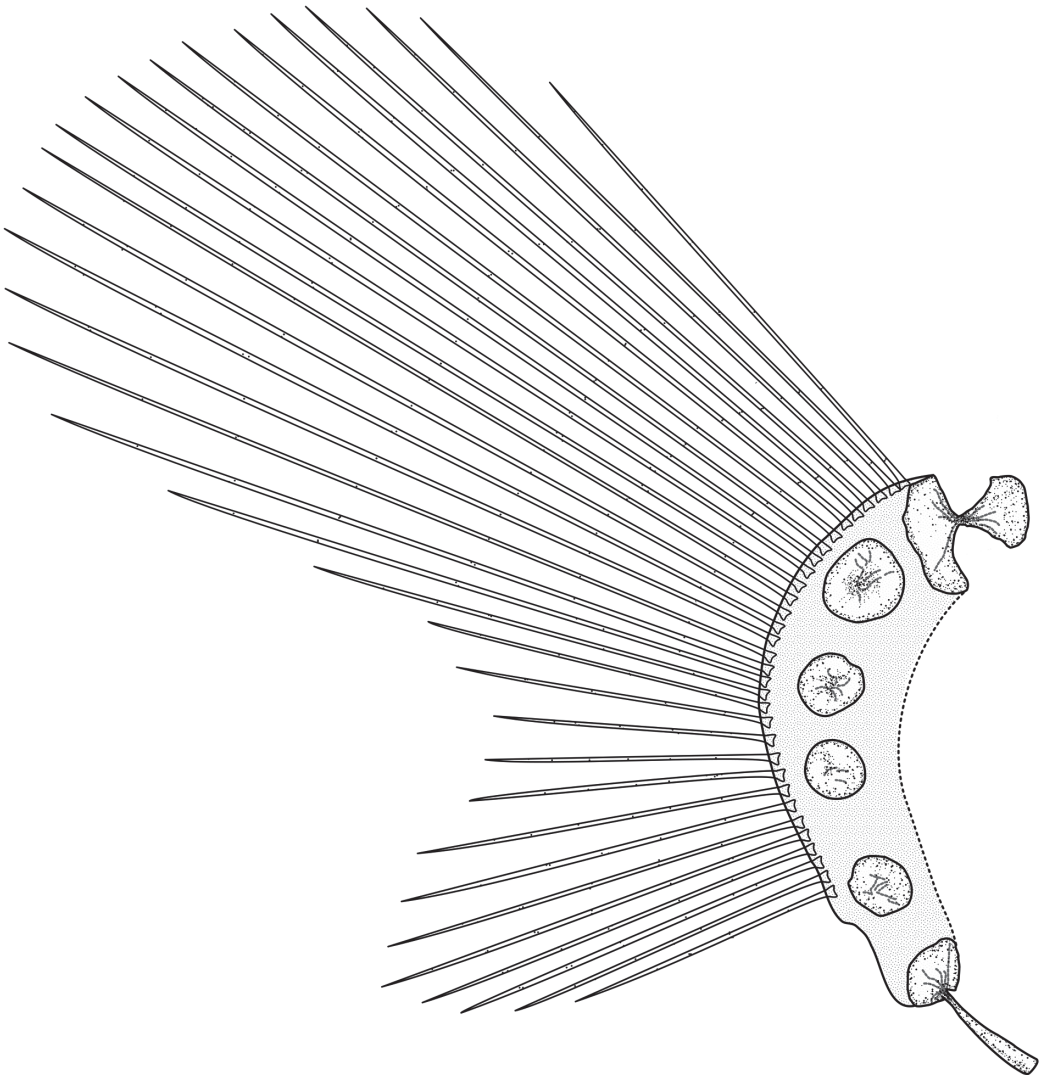

FIGURE 5. Pectoral girdle of USNM 438994/HADES 200027, female, 220 mm. Ventral drawing of USNM 438995/HADES 200085, female, 225 mm. Scapula, radials 1–4, coracoid shown. Drawing by Thomas D. Linley.

TABLE 2. Measurements and counts of *Pseudoliparis swirei* **sp. nov.**. Measurements taken from preserved specimens, given in mm. Body depth measured from fresh photographs. Dorsal fin origin between vertebrae #, # are shown. Maximum and minimum values (mean and standard deviation) shown for measurements. Counts show range (median). Number of specimens examined for individual characters (*n*).

	Holotype	Holotype and Paratypes	n
Measurements			
Standard Length	104.0	87.0–226.0 (151.3±38.8)	24
Total Length	112.0	95.0–237.0 (160.5±41.6)	21
Head Length	18.9	17.8–42.9 (31.2±8.0)	20
Head Depth at Occiput	~14	20.5–32.7 (27.3±6.2)	3
Head Width	13.1	2.6–41.4 (27.0±9.7)	11
Snout Length	6.7	5.6–15.2 (9.8±2.8)	26
Lower Lobe Distance		2.3–6.6 (4.7±1.4)	16
Body Depth	18.0	18.0–62.0 (41.0±11.0)	18
Orbit Width	3.5	2.8–6.1 (4.8±1.0)	23
Disk Length		2.9–9.0 (6.2±2.1)	14
Gill Opening		5.4–9.6 (8.1±2.4)	3
Upper Jaw Length	~8.7	8.1–20.6 (13.8±3.3)	31
Lower Jaw Length	8.2	6.6–19.3 (12.7±3.1)	31
Distance: Mandible to Disk	8.8	8.8–22.3 (15.2±3.7)	25
Distance: Snout to Anus	23.2	23.2–56.7 (41.1±13.5)	6
Distance: Mandible to Anus	21.0	21.0–47.5 (35.3±12.0)	5
Distance: Disk to Anus	9.5	9.5–33.5 (18.7±8.9)	5
Distance: Anus to Anal Fin	10.9	10.9–25.9 (18.4±6.3)	7
Length Upper Pectoral Fin Lobe	>15.6	14.2–33.4 (22.8±4.5)	28
Length Lower Pectoral Fin Lobe	8.9	7.3–22.9 (12.3±3.3)	22
Counts			
Total Vertebrae	58	56–62 (59)	19
Abdominal Vertebrae	12	11–14 (12)	18
Caudal Vertebrae	46	44–49 (46)	17
Dorsal Fin Origin		3–6 (4,5)	12
Dorsal Fin Rays	~52	51–58 (54)	11
Anal Fin Rays	≥44	43–49 (47)	15
Total Pectoral Rays	30	28–32 (30)	24
Pectoral Fin Rays (Upper Lobe)	20	18–23 (21)	26
Pectoral Rays (Notch)	5	3–6 (5)	27
Pectoral Fin Rays (Lower Lobe)	5	4–6 (5)	26
Total Caudal Fin Rays	13	11–14 (13)	20
Caudal Fin Rays (Upper)	5	4–6 (5)	21
Caudal Fin Rays (Lower)	6	4–7 (6)	21
Caudal Fin Rays (Auxiliary)	2	0–2 (1)	20
Pyloric Caeca		5–9 (7)	17

TABLE 3. Ratios of *Pseudoliparis swirei* **sp. nov.**. Preserved and fresh measurements presented. Body depth taken from photographs. Predorsal fin length measured from radiograph.

	%SL			%HL		
	Holotype	Holotype and Paratypes	n	Holotype	Holotype and Paratypes	n
Preserved						
Head Length	18.2	17.0–21.7 (19.8±1.1)	19			
Head Width	12.6	12.6–19.6 (15.8±2.5)	8	69.3	68.2–101.0 (81.0±11.5)	8
Snout Length	6.4	5.2–8.3 (6.5±0.7)	21	35.4	28.5–38.0 (32.9±2.6)	18
Orbit Width	3.4	2.3–4.4 (3.2±0.6)	17	18.5	12.1–20.1 (16.0±2.3)	16
Upper Jaw Length	~8.4	7.4–10.5 (9.1±0.8)	20	~46.0	38.3–52.2 (45.9±3.3)	17
Lower Jaw Length	7.9	6.5–10.6 (8.3±1.0)	20	43.4	33.7–53.2 (42.2±4.7)	17
Upper Pectoral Fin Length		12.6–19.8 (15.2±2.2)	21		60.2–95.4 (75.4±11.3)	16
Lower Pectoral Fin Length	8.6	6.3–12.1 (7.8±1.4)	16	47.1	30.0–61.6 (39.0±7.7)	14
Gill Opening		4.4–5.3 (5.0±0.5)	3		22.3–26.5 (24.9±2.3)	3
Disk Length		2.4–5.6 (3.9±0.9)	13		12.1–25.9 (20.0±4.0)	12
Distance: Disk to Anus	9.1	8.6–15.6 (10.8±3.2)	4	50.3	43.1–83.8 (59.0±21.7)	3
Distance: Mandible to Disk	8.5	7.7–13.7 (10.0±1.4)	20	46.6	39.8–59.8 (49.7±5.4)	17
Lower Lobe Distance		1.8–4.7 (3.1±0.9)	12		8.3–23.0 (15.2±4.7)	10
Predorsal Fin Length	32.0	22.7–32.6 (27.8±3.1)	13	176.4	118.1–176.4 (142.2±18.2)	13
Distance: Snout to Anus	22.3	22.3–29.3 (26.0±3.0)	6	122.8	114.6–143.3 (130.0±11.3)	5
Distance: Mandible to Anus	20.2	20.2–27.6 (24.3±3.4)	4	111.1	111.1–134.8 (120.1±12.8)	3
Distance: Anus to Anal Fin	10.5	8.7–15.9 (12.5±2.9)	5	57.7	46.5–66.6 (59.1±9.3)	4
Fresh						
Head Length	20.6	14.5–21.9 (18.7±1.8)	33			
Snout Length	7.2	4.3–9.3 (6.4±1.0)	33	35.0	26.3–45.5 (33.8±5.3)	37
Eye Width	2.1	0.9–2.9 (1.8±0.5)	33	10.0	5.3–15.4 (9.9±2.4)	37
Body Depth	18.6	18.6–31.2 (24.5±3.1)	18	90.0	90.0–156.8 (128.7±17.9)	18
Preanal Fin Length	37.1	36.5–49.5 (42.0±3.5)	33	180.0	180.0–295.8 (228.0±26.1)	37

Disk present, oval, longer than wide, below cheek and gill cavity between pectoral fin notches; well behind pectoral symphysis. Bones fully developed but weakly calcified; all elements present. Disk and pectoral girdle supported by a pair of clearly visible and strongly developed muscles extending anteriorly to pectoral symphysis, probably infracarinalis anterior (D.L. Stein, *personal communication*). Disk structure supporting a thin layer of tissue, often damaged or missing entirely; disk margin only slightly thicker than more central tissue. In cross section, disk rays clearly flattened as if to support disk margin.

Body depth dependent on reproductive state and fullness of stomach, usually much deeper than head depth, but shallow above vertebral column. Abdominal cavity long; peritoneum and body cavity extending to about 40% standard length. Total vertebrae 61 (56–62); anterior 13 (11–14), caudal 46 (44–49). In the 19 individuals in good enough condition to be radiographed, a double ray is present at or near anal fin first ray, usually between the second and third haemal spines of the caudal vertebrae. Pre-dorsal length about 27% SL (18.6–32.6), dorsal fin origin between fourth and fifth vertebrae (origin after vertebrae 3–5). Pre-anal-fin length about 42% SL (36.3–49.5)*. Anus far posterior to disk, roughly 2/3 of distance from disk to anal fin origin. Pyloric caeca usually 7 (5–9), located left ventrally in body cavity; thick, digitate, usually separated into two distinct size classes, most commonly 4 short and 3 long, longest about 8.7% SL (5.9–11.7), shortest 3.7% SL (2.4–5.3). Longer caeca generally grouped together. Hypural with obvious suture; caudal fin most commonly of 13 (11–14) rays, ventral one or two often rudimentary. Skin thin, transparent; subdermal extracellular matrix (SECM; Eastman *et al.* 1994) thick below skin

and between muscle bands. Total and standard lengths were approximately 10% shorter after preservation. The subdermal extracellular matrix is also lost after capture and preservation, resulting in changes to shape and proportion (Gerringer *et al.* unpublished data). With increased use of visual *in situ* techniques, reporting of both fresh and preserved specimen features will become increasingly useful.

The 37 individuals used for description varied in size from 89–235 mm SL, apparently covering a wide developmental range for the species. Some characters correlated significantly with ontogeny, explaining much of the variation in ratios. Both the upper and lower pectoral-fin lobe lengths as a percentage of SL decreased significantly with increasing SL (upper: $F_{1,25}$=11.88, $p<0.01$, R^2=0.322; lower $F_{1,23}$=5.05, $p<0.05$, R^2=0.180). Proportional orbit width decreased with increasing standard length ($F_{1,18}$=26.25, $p<0.01$, R^2=0.593).

In life, body pinkish-white, skin and peritoneum transparent; internal organs (liver, stomach, pyloric caeca) and muscles of trunk clearly visible through skin and thin abdominal wall. Anterior bundles of epaxial muscle thick, becoming less densely packed posteriorly. Some larger specimens with dusky skin on head. Pyloric caeca orange; most individuals entirely lacked both internal and external pigmentation. In alcohol, except for those with dusky heads, specimens uniformly pale.

Phylogenetic inference supports placement within the genus *Pseudoliparis*, with *P. swirei* **sp. nov.** more closely related to *P. belyaevi* of the Japan Trench than to the Kermadec Trench liparids (*Notoliparis kermadecensis*; *N. stewarti*). Phylogenetic relationships of *P. swirei* **sp. nov.** and closely-related species based on 16S, COI, and Cyt-*b* are presented in Figure 6, with estimates of evolutionary divergence among species reported in Table 4. Both the 16S and Cyt-*b* trees support placement of *P. swirei* **sp. nov.** as most closely related to *P. belyaevi* (>74% ML bootstrap support, >0.96 Bayesian posterior probability), with highly concordant topology. Genetic distances between the two species of *Pseudoliparis* are 0.6% at Cyt-*b* and 0.7% at 16S rRNA (Table 4), with distances of 1–1.4% (Cyt-*b*) and 0.8–1% (16S rRNA) to the *Notoliparis* species. COI lacked sufficient polymorphism to resolve the relevant nodes, with low bootstrap support observed for the placement of *P. swirei* **sp. nov.** relative to P. *belyaevi* and *N. kermadecensis* (Figure 6). Genetic distances among species also were the lowest at COI, at <1% or three nucleotide substitutions observed between the sequences of *Pseudoliparis*. Phylogenetic analyses conducted using the more closely-related *Careproctus* outgroup taxa, but with a shorter alignment (696-bp 16S rRNA, 744-bp Cyt-*b*, 645-bp COI) found congruent results to the trees presented in Figure 6 (*Aptocyclus* outgroup), but with lower bootstrap support for most nodes (Supplementary Figure 2). The 16S rRNA phylogeny supported placement of the new species into *Pseudoliparis* (67% ML bootstrap support/0.75 Bayesian posterior probability), and moderate support was observed at Cyt-*b* (0.82 Bayesian posterior probability, ML unresolved). There was still no significant resolution of generic placement in the COI phylogeny with the *Careproctus* outgroup species. Sequences from *Pseudoliparis swirei* **sp. nov.**, *Notoliparis kermadecensis, Notoliparis stewarti* (this study) are available under GenBank accession numbers KY659176–KY659204 (Supplementary Table 2).

Reproduction. Holotype is immature. Ripe females had eggs up to 9.4 mm diameter, among the largest teleost eggs recorded (Tyler and Sumpter, 1996), 0.4 mm smaller than the largest record (Matallanas *et al.*, 1990). The eggs were unsorted within gonad, with the largest eggs free and interspersed within a matrix of smaller eggs. No developmental structures were visible within even the largest eggs. Two distinct size classes of eggs present with up to 23 large eggs (>5 mm) and up to 851 small eggs of less than half the diameter of the larger size class. There were rarely intermediate stages (Figure 7). Individuals with only small eggs had maximum egg sizes ranging from 0.7 to 1.4 mm. Genital papilla visible in freshly collected males, oriented anteriorly.

Distribution. Known only from the Mariana Trench at capture depths from 6,898–7,966 m, individuals likely this species were recognized in video at depths 6,198–8,098 m (Linley *et al.* 2016; Jamieson & Linley, unpublished data).

Etymology. The Mariana Trench famously houses the ocean's deepest point, at Challenger Deep, named for the *HMS Challenger* expedition which discovered the trench in 1875. Their deepest sounding of 8,184 m, then the greatest known ocean depth, was christened Swire Deep after Herbert Swire, the ship's First Navigating Sublieutenant (Corfield 2003). We name this fish in his honor, in acknowledgment and gratitude of the crew members that have supported oceanographic research throughout history.

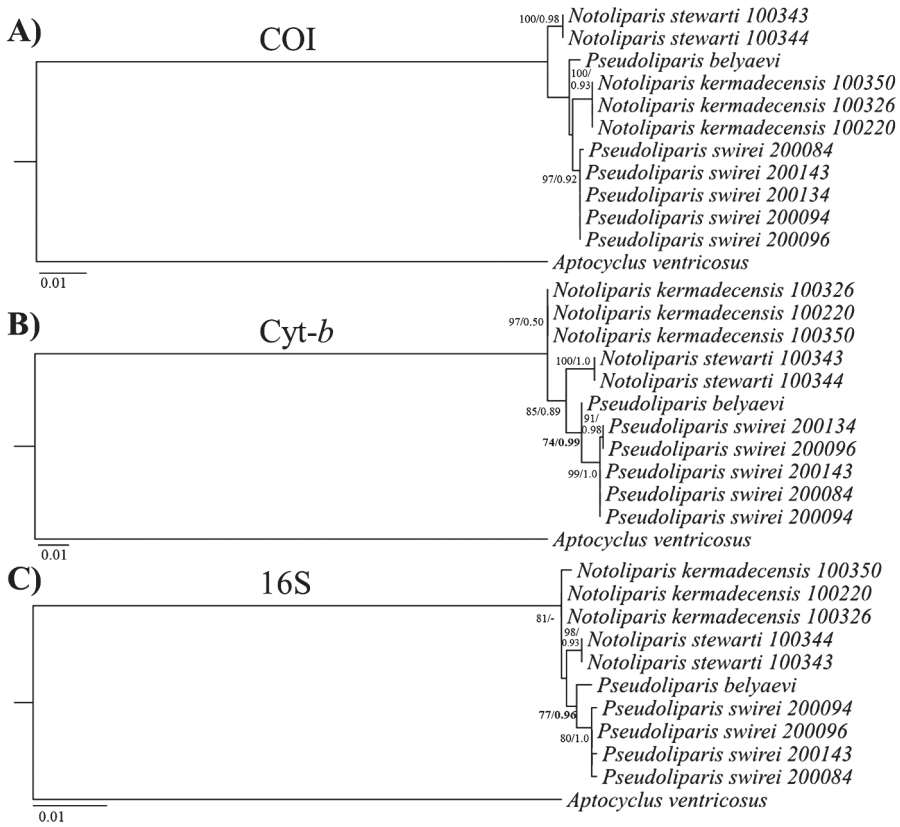

FIGURE 6. Phylogenetic relationships of *Pseudoliparis swirei* **sp. nov.** to closely related hadal liparids, *P. belyaevi* from the Japan Trench and *Notoliparis kermadecensis* and *Notoliparis stewarti* from the Kermadec Trench. Maximum likelihood (ML) trees based on A) cytochrome *c* oxidase subunit I (1399 bp), B) cytochrome *b* (1007 bp), and C) 16S rRNA (1472 bp). ML bootstrap support (>70%) and Bayesian posterior probability (>0.70) values are shown as ML/BI. Bold values indicate the node that supports placement of *P. swirei* **sp. nov.** within the genus *Pseudoliparis*. *Aptocyclus ventricosus* (GenBank accession NC008129.1) was used to root each tree.

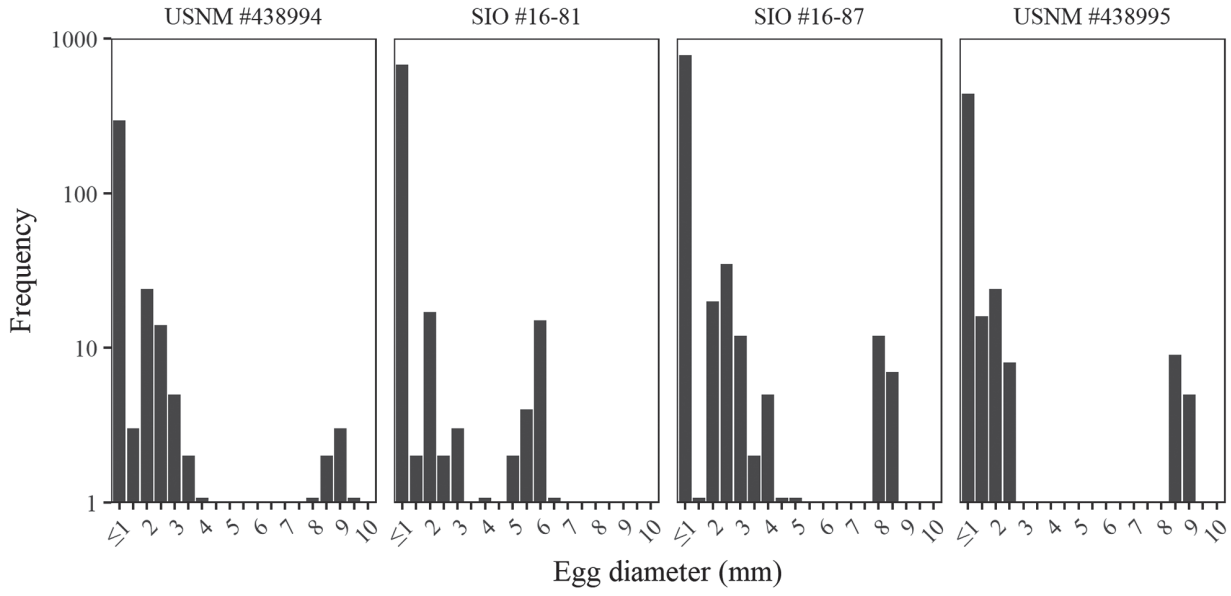

FIGURE 7. Egg sizes and frequencies from four individuals. Binned into 0.5 mm increments. Small peaks show 22, 23, 7, 14 large eggs for specimens USNM 438994/HADES 200027, SIO 16-81/HADES 200039, SIO 16-87/HADES 200025, USNM 438995/HADES 200085.

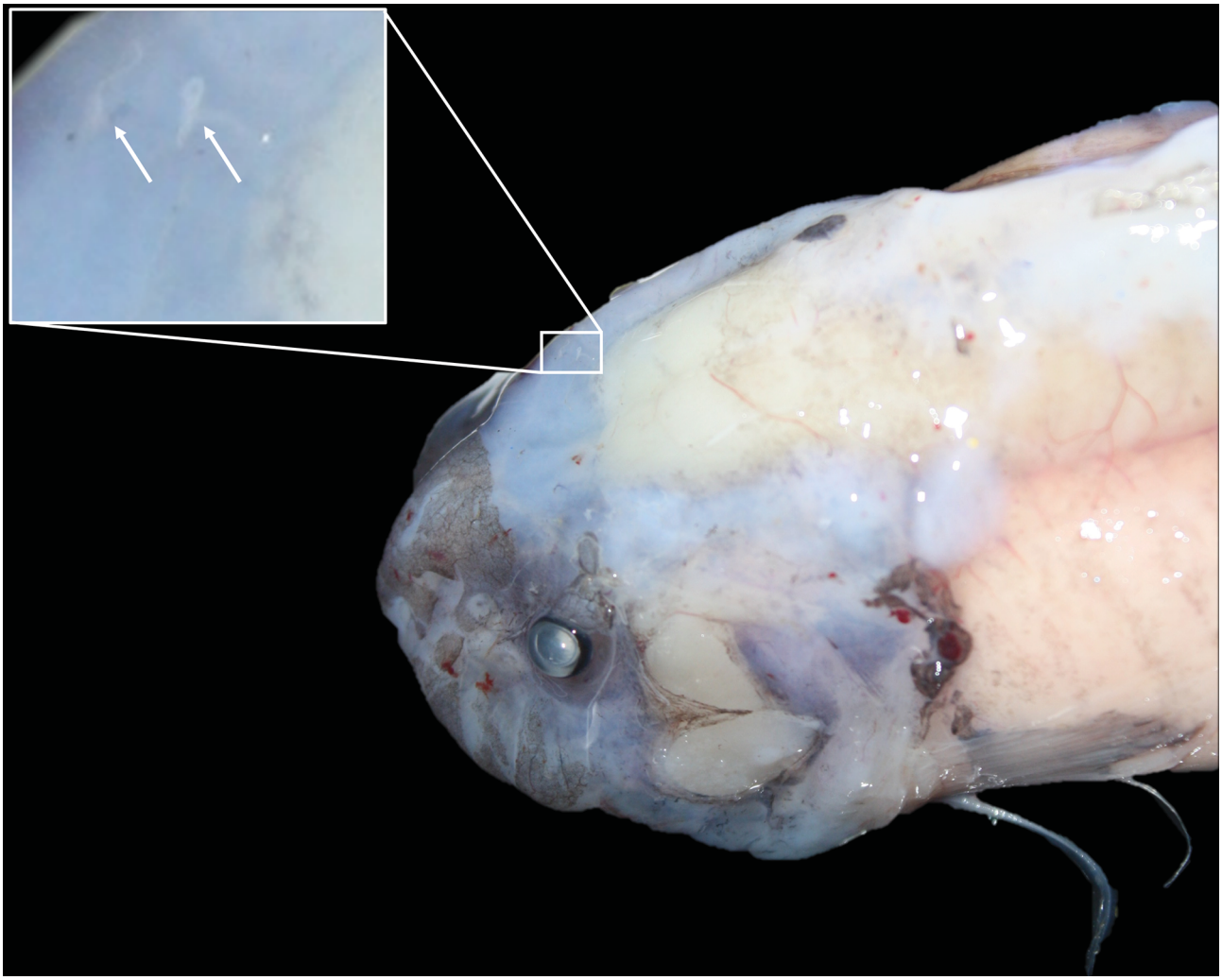

FIGURE 8. Postcoronal pores in freshly-caught specimen. Paratype TUMSAT 30670/SY1615028, male, head length 45 mm.

Discussion

Currently, the hadal liparid genera *Notoliparis* (Andriashev, 1975) and *Pseudoliparis* (Andriashev, 1955) are distinguished from one another only by the presence in the former (and absence in the latter) of a series of "extra" postcoronal and temporal cephalic pores (Andriashev & Pitruk, 1993). These pores are easily damaged or lost during sampling and recovery of specimens, in which case it is impossible to determine to which genus a specimen should be assigned. Andriashev himself noted that in at least one species of *Notoliparis*, *N. macquariensis* (Andriashev, 1978), the tiny posterior pores were only briefly visible in freshly caught specimens (Andriashev 1978). Due to the fragile skin and time spent in warm (up to 30°C) surface waters during recovery, very few of these pores remained in our material. In one individual (SY1615028), two postcoronal pores were visible (Figure 8). However, the skin had been damaged in such a way that temporal cephalic pores were lost. Other characters distinguishing the two genera overlap and cannot be used to assign a species to genus.

Given the uncertainty of the pore observations and without strong morphological justification for placement in either genus, we assign this new species to the genus *Pseudoliparis* on genetic grounds. Phylogenetic analyses supported a closer relationship between *P. swirei* **sp. nov.** and *Pseudoliparis belyaevi* in the Japan Trench than to hadal liparid populations in the Kermadec Trench (*N. kermadecensis*, *N. stewarti*; Table 4, Figure 6). Our molecular results also supported the distinction of two hadal liparid species in the Kermadec Trench as described by Stein (2016), *Notoliparis kermadecensis* and *Notoliparis stewarti*, which appear to have overlapping distributions.

TABLE 4. Evolutionary divergence between *Pseudoliparis swirei* sp. nov. and close relatives. Average genetic distance among species calculated for (A) cytochrome *c* oxidase subunit I (644 bp), (B) cytochrome b (744 bp), and (C) 16S rRNA (699 bp), based on the Tamura-Nei substitution model with gamma-distributed rate variation across sites. Sequences from *P. swirei* sp. nov., *N. kermadecensis, N. stewarti* derive from this study, *P. belyaevi* are unpublished data from T. Satoh (National Museum of Nature and Science, Japan), sequences from *C. rastrinus, C. cypselurus, A. ventricosus* were from NCBI (GenBank Accession Numbers: AB565515.1, AB565517.1, AB565629.1, FJ164433.1, JF952697.1, NC_008129.1).

COI	*Aptocyclus ventricosus*	*Careproctus cypselurus*	*Careproctus rastrinus*	*Notoliparis kermadecensis*	*Notoliparis stewarti*	*Pseudoliparis belyaevi*	*Pseudoliparis swirei* sp. nov.
Aptocyclus ventricosus	***						
Careproctus cypselurus	0.648	***					
Careproctus rastrinus	0.505	0.173	***				
Notoliparis kermadecensis	0.359	0.121	0.139	***			
Notoliparis stewarti	0.353	0.121	0.138	0.01	***		
Pseudoliparis belyaevi	0.391	0.12	0.136	0.009	0.015	***	
Pseudoliparis swirei sp. nov.	0.373	0.13	0.133	0.004	0.01	0.005	***

Cyt-b	*Aptocyclus ventricosus*	*Careproctus colletti*	*Careproctus rastrinus*	*Notoliparis kermadecensis*	*Notoliparis stewarti*	*Pseudoliparis belyaevi*	*Pseudoliparis swirei* sp. nov.
Aptocyclus ventricosus	***						
Careproctus colletti	1.026	***					
Careproctus rastrinus	0.881	0.196	***				
Notoliparis kermadecensis	0.742	0.245	0.193	***			
Notoliparis stewarti	0.813	0.216	0.189	0.015	***		
Pseudoliparis belyaevi	0.769	0.241	0.179	0.01	0.01	***	
Pseudoliparis swirei sp. nov.	0.779	0.237	0.189	0.014	0.014	0.006	***

16S	*Aptocyclus ventricosus*	*Careproctus rastrinus*	*Notoliparis kermadecensis*	*Notoliparis stewarti*	*Pseudoliparis belyaevi*	*Pseudoliparis swirei* sp. nov.
Aptocyclus ventricosus	***					
Careproctus rastrinus	0.3	***				
Notoliparis kermadecensis	0.271	0.075	***			
Notoliparis stewarti	0.281	0.075	0.003	***		
Pseudoliparis belyaevi	0.281	0.072	0.008	0.008	***	
Pseudoliparis swirei sp. nov.	0.303	0.08	0.01	0.01	0.007	***

Our results also call into question the genus-level distinction between hadal liparids of *Pseudoliparis* and *Notoliparis*. The close genetic similarities between species of *Pseudoliparis* and *Notoliparis*, the fleeting and dubious nature of the distinguishing character of cephalic pores, and the behavioral and morphological consistencies between the two genera make it difficult to justify a division between these two groups. Aside from cephalic pore counts, the two genera overlap in meristic characters and counts (Stein 2016; Andriashev & Pitruk 1993). Further, in ecological studies, hadal liparids seem to fill very similar niches in their respective trenches (Jamieson *et al.* 2009; Fujii *et al.* 2010; Linley *et al.* 2016; Linley *et al.* 2017; Gerringer *et al.* 2017a). Synonymizing these two hadal genera should be considered when genetic information on a greater number of species of *Notoliparis* and *Pseudoliparis* become available.

Pseudoliparis swirei **sp. nov.** was abundant at depths of approximately 7,000–8,000 m in the Mariana Trench. Video records showed large aggregations of different-sized individuals were attracted to the bait (Linley *et al.* 2016) and fed on swarms of amphipods that also arrived (Linley *et al.* 2017; Gerringer *et al.* 2017a). Smaller individuals were caught at greater depths (Linley *et al.* 2016). No individuals were seen at depths below 8,200 m, which is hypothesized to be the physiological depth limit for teleosts (Yancey *et al.* 2014). The discovery of yet another trench liparid species provides further evidence for the importance of this family within the hadal environment. This collection will allow further exploration of hadal endemism and the factors leading to the recurrent colonization of trenches by liparids.

Material examined

Holotype. USNM 438975/HADES 200060, immature, 104/97* mm SL, Stn. WT06, 12.3037°N, 144.6804°E, 7949 m, 21 Nov 2014.

Paratypes. USNM 438993/HADES 200021, male, ~184/193* mm SL, Stn. TR05, 12.5979°N, 144.7785°E, 7062 m, 15 Nov 2014. USNM 438996/HADES 200024, sex unknown, 232* mm SL, SIO 16-87/HADES 200025, female, 226/235* mm SL, Stn. WT03, 12.6103°N, 144.7684°E, 6961 m, 16 Nov 2014. USNM 438994/HADES 200027, female, 220* mm SL, Stn. TR06, 12.6339°N, 144.7508°E, 6914 m, 16 Nov 2014. USNM 438997/HADES 200033, sex unknown, ~170 mm SL, Stn. WT04, 12.4151°N, 144.9119°E, 7495 m, 18 Nov 2014. USNM 438991/HADES 200036, sex unexamined, 186* mm SL, USNM 438976/HADES 200037, sex unexamined, 87/89* mm SL, SIO 16-81/HADES 200038, sex unexamined, 163/165* mm SL, SIO 16-81/HADES 200039, female, 211/210* mm SL, USNM 438990/HADES 200040, female, 181/184* mm SL, USNM 438977/HADES 200041, sex unknown, 107/105* mm SL, SIO 16-81/HADES 200042, sex unknown, 142/147* mm SL, SIO 16-81/HADES 200043, female, 182 mm, Stn. TR07, 12.4235°N, 144.8706°E, 7497 m, 18 Nov 2014. USNM 438988/HADES 200047, male, 169/178* mm SL, USNM 438983/HADES 200048, male, 135+* mm SL, SIO 16-82/HADES 200049, 123/128* mm SL, USNM 438998/HADES 200050, sex unexamined, ~100 mm SL, Stn. TR08, 12.4256°N, 144.9117°E, 7509 m, 19 Nov 2014. SIO 16-83/HADES 200062, sex unknown, 16* mm head length Stn. TR09, 12.3027°N, 144.6739°E, 7929 m, 21 Nov 2014. SIO 16-84/HADES 200070, female, 163/172* mm SL, USNM 438978/HADES 200071, sex unknown, 111/110* mm SL, USNM 438979/HADES 200072, juvenile, ~115/119* mm SL, Stn. TR10, 11.9128°N, 144.9445°E, 7841 m, 23 Nov 2014. USNM 438984/HADES 200074, male, 139/145* mm SL, Stn. WT07, 11.9273°N, 144.9620°E, 7907 m, 23 Nov 2014. SIO 16-88/HADES 200081, juvenile, >103/107* mm SL, Stn. WT08, 11.9297°N, 144.9288°E, 7966, 24 Nov 2014. USNM 438987/HADES 200084, female, 176* mm SL, USNM 438995/HADES 200085, female, 215/225* mm SL, Stn. WT09, 11.8147°N, 144.9858°E, 6949 m, 25 Nov 2014. SIO 16-85/HADES 200087, female, ~192/203* mm SL, Stn. TR12, 11.8107°N, 144.9945°E, 6898 m, 25 Nov 2014. USNM 438992/HADES 200094, female, 178/187* mm SL, USNM 438981/HADES 200095, female, 123/124* mm SL, USNM 438989/HADES 200096, female, >173/183* mm SL, Stn. TR13, 11.8260°N, 145.0088°E, 6974, 26 Nov 2014. USNM 438985/HADES 200133, juvenile, 143/151* mm SL, USNM 438986/HADES 200134, female, 155/161* mm SL, Stn. TR19, 12.2766°N, 144.6202°E, 7626 m, 6 Dec 2014. SIO 16-86/HADES 200141, sex unexamined, 132/139* mm SL, SIO 16-86/HADES 200142, male, 138/142* mm SL, USNM 438982/HADES 200143, female, 119/129* mm SL, USNM 438980/HADES 200144, juvenile, 112/119* mm SL, Stn. TR20, 12.3495°N, 144.6813°E, 7652 m, 7 Dec 2014. TUMSAT 30670/SY1615028, male, 208/213* mm SL, Stn. FT02, 11.5429°N, 142.1849°E, 7581 m, 29 Jan 2017. SL measured preserved/fresh* for all.

Acknowledgements

This work was supported by the National Science Foundation Grant OCE #1130712, Schmidt Ocean Institute, and the Marine Alliance for Science and Technology for Scotland (MASTS). We are extremely grateful to T.P. Satoh (National Museum of Nature and Science, Japan) for providing *P. belyaevi* genetic data. The authors also express their gratitude to the NOAA Monument office for access to the Marianas Trench Marine National Monument, D. Stein (Oregon State University) for access to literature and taxonomic consultation, N. Chernova (ZIN) for access to Russian literature, S. Raredon (Smithsonian Institution) for obtaining radiographs of the specimens, Marilyn Dunlap and Tina Carvalho for providing dyes (University of Hawai'i), Shaobin Hou and Xuehua Wan (University of Hawai'i) for DNA sequencing, Adam Summers (University of Washington) for microCT images and the 3D model at the Karel F. Liem BioImaging Center, the Government of the Federated States of Micronesia for specimen collection permissions, and the University of Guam for assistance in acquiring chemicals. G. Shinohara, National Museum of Nature and Science, Tokyo, loaned specimens of *P. amblystomopsis*. M. Gerringer is grateful for the support of NSF's Graduate Research Fellowship Program. T. Linley and A. Jamieson are supported by, and extend their thanks to, the MASTS pooling initiative. The MASTS Postdoctoral and Early Career Researcher Exchanges (PECRE) also supported T. Linley's travel expenses without which direct work on the specimens would not have been possible. We thank NOAA-NMFS Pacific Islands Fisheries Science Center, the Pacific Islands Regional Office, the Marine National Monuments Program, and E. Breuer (NOAA/NMFS), and NHK Japan Broadcasting Corporation for their assistance and collaboration. We extend also our heartfelt thanks to the captains and crews of the *R/V Falkor* and *R/V Shinyo-maru*, and participants in the HADES (HADal Ecosystems Studies) Program. This is SOEST contribution #10267.

References

Andriashev, A. (1978) On the third species of the ultra-abyssal genus *Notoliparis* Andr. (Pisces. Liparidae), from the deepwaters of the Macquarie Trench, with some notes on zoogeographic and evolutionary significance of this discovery. *Trudy Instituta Okeanologii Akad. Nauk. SSSR,* 112, 152–161.

Andriashev, A. (2003) Snailfishes (Liparidae, Scorpaeniformes) from the Southern Ocean and adjacent waters. *In: Issledovaniya fauny morei (Study of Marine Fauna) St. Petersburg: Zool. Inst., Ross. Akad. Nauk*.

Andriashev, A.P. & Pitruk, D.L. (1993) A review of the ultra-abyssal (hadal) genus *Pseudoliparis* (Scorpaeniformes, Liparidae) with a description of a new species from the Japan Trench. *Voprosy ikhtiologii,* 33, 325–330.

Chernova, N., Stein, D. & Andriashev, A. (2004) Family Liparidae Scopoli 1777. *California Academy of Sciences Annotated Checklists of Fishes* 31.

Corfield, R. (2003) *The Silent Landscape the Scientific Voyage of HMS Challenger*. Washington, D.C.: Joseph Henry Press, Washington, D.C., 285 pp.

Darriba, D., Taboada, G.L., Doallo, R. & Posada, D. (2012) jModelTest 2: more models, new heuristics, and parallel computing. *Nature Methods,* 9 (8), 772.
https://doi.org/10.1038/nmeth.2109

Eastman, J., Hikida, R. & Devries, A. (1994) Buoyancy studies and microscopy of skin and subdermal extracellular matrix of the antarctic snailfish, *Paraliparis devriesi*. *Journal of Morphology,* 220, 85–101.
https://doi.org/10.1002/jmor.1052200108

Edgar, R.C. (2004) MUSCLE: Multiple sequence alignment with high accuracy and high throughput. *Nucleic Acids Research,* 32, 1792–1797.
https://doi.org/10.1093/nar/gkh340

Fujii, T., Jamieson, A., Solan, M., Bagley, P. & Priede, I. (2010) A large aggregation of liparids at 7703 meters and a reappraisal of the abundance and diversity of hadal fish. *BioScience*, 60, 506–515.
https://doi.org/10.1525/bio.2010.60.7.6

Gerringer, M.E., Popp, B.N., Linley, T.D., Jamieson, A.J. & Drazen, J.C. (2017a) Comparative feeding ecology of abyssal and hadal fishes through stomach content and amino acid isotope analysis. *Deep-Sea Research Part I: Oceanographic Research Papers* 121, 110–120.
https://doi.org/10.1016/j.dsr.2017.01.003

Gerringer, M.E., Drazen, J.C. & Yancey, P.H. (2017b) Metabolic enzyme activities of abyssal and hadal fishes: pressure effects and a re-evaluation of depth-related changes. *Deep-Sea Research Part I: Oceanographic Research Papers,* 125, 135–146.
https://doi.org/10.1016/j.dsr.2017.05.010

Guindon, S. & Gascuel, O. (2003) A simple, fast, and accurate method to estimate large phylogenies by maximum-likelihood. *Systematic Biology* 52, 696–704.

https://doi.org/10.1080/10635150390235520
Hay, D.E. (1982) Fixation shrinkage of herring larvae: Effects of salinity, formalin concentration, and other factors. *Canadian Journal of Fisheries and Aquatic Sciences* 39, 1138–1143.
https://doi.org/10.1139/f82-151
Jamieson, A.J., Fujii, T., Solan, M., Matsumoto, A.K., Bagley, P.M. & Priede, I.G. (2009) Liparid and macrourid fishes of the hadal zone: *in situ* observations of activity and feeding behaviour. *Proceedings of the Royal Society B: Biological Sciences,* 276 (1659), 1037–1045.
https://doi.org/10.1098/rspb.2008.1670
Jamieson, A.J., Kilgallen, N., Rowden, A., Fujii, T., Horton, T., Lörz, A.-N., Kitazawa, K. & Priede, I. (2011) Bait-attending fauna of the Kermadec Trench, SW Pacific Ocean: Evidence for an ecotone across the abyssal–hadal transition zone. *Deep Sea Research Part I: Oceanographic Research Papers* 58, 49–62.
https://doi.org/10.1016/j.dsr.2010.11.003
Kai, Y., Orr, J.W., Sakai, K. & Nakabo, T. (2011) Genetic and morphological evidence for cryptic diversity in the *Careproctus rastrinus* species complex (Liparidae) of the North Pacific. *Ichthyological Research,* 58, 143–154.
https://doi.org/10.1007/s10228-010-0202-2
Kearse, M., Moir, R., Wilson, A., Stones-Havas, S., Cheung, M., Sturrock, S., Buxton, S., Cooper, A., Markowitz, S., Duran, C., Thierer, T., Ashton, B., Mentjies, P. & Drummond, A. (2012) Geneious Basic: an integrated and extendable desktop software platform for the organization and analysis of sequence data. *Bioinformatics,* 28 (12), 1647–1649.
https://doi.org/10.1093/bioinformatics/bts199
Kristoffersen, J.B. & Salvanes, A.G.V. (1998) Effects of formaldehyde and ethanol preservation on body and otoliths of *Maurolicus muelleri* and *Benthosema glaciale*. *Sarsia,* 83, 95–102.
https://doi.org/10.1080/00364827.1998.10413675
Letunic, I. & Bork, P. (2007) Interactive Tree of Life (iTOL): an online tool for phylogenetic tree display and annotation. *Bioinformatics* 23, 127–8.
https://doi.org/10.1093/bioinformatics/btl529
Linley, T.D., Gerringer, M.E., Yancey, P.H., Drazen, J.C., Weinstock, C.L. & Jamieson, A.J. (2016) Fishes of the hadal zone including new species, *in situ* observations and depth records of Liparidae. *Deep Sea Research Part I: Oceanographic Research Papers,* 114, 99–110.
https://doi.org/10.1016/j.dsr.2016.05.003
Linley, T.D., Stewart, A.L., McMillan, P.J., Clark, M.R., Gerringer, M.E., Drazen, J.C., Fujii, T. & Jamieson, A.J. (2017) Bait attending fishes of the abyssal zone and hadal boundary: community structure, functional groups and species distribution in the Kermadec, New Hebrides and Mariana trenches. *Deep Sea Research Part I: Oceanographic Research Papers,* 121, 38–53.
https://doi.org/10.1016/j.dsr.2016.12.009
Matallanas, J., Rucabado, J., Lloris, D. & Olivar, M.P. (1990) Early stages of development and reproductive biology of the South-American eelpout *Austrolycus depressiceps* Regan, 1913 (Teleostei: Zoarcidae). *Scientia Marina*, 54 (3), 257–261.
McWilliam, H., Li, W., Uludag, M., Squizzato, S., Park, Y.M., Buso, N., Cowley, A.P. & Lopez, R. (2013) Analysis Tool Web Services from the EMBL-EBI. *Nucleic Acids Research,* 41, 597–600.
https://doi.org/10.1093/nar/gkt376
Miya, M., Takeshima, H., Endo, H., Ishiguro, N.B., Inoue, J.G., Mukai, T., Satoh, T.P., Yamaguchi, M., Kawaguchi, A., Mabuchi, K., Shirai, S.M. & Nishida, M. (2003) Major patterns of higher teleostean phylogenies: a new perspective based on 100 complete mitochondrial DNA sequences. *Molecular Phylogenetics and Evolution,* 26 (1), 121–138.
https://doi.org/10.1016/S1055-7903(02)00332-9
Pérês, J. (1965) Aperçu sur les résultats de deux plongées effectuées dans le ravin de Puerto-Rico par le bathyscaphe Archimède. *Deep-Sea Research and Oceanographic Abstracts,* 12, 883–891.
https://doi.org/10.1016/0011-7471(65)90811-9
R Core Development Team (2015) R: A Language and Environment for Statistical Computing. *R Foundation for Statistical Computing* Vienna, Au.
Sabaj Perez, M. (2014) Standard Symbolic Codes for Institutional Resource Collections in Herpetology and Ichthyology Citation. Version 5.
Saruwatari, T., López, J.A., Pietsch, T.T.W., Lopez, J. & Pietsch, T.T.W. (1997) Cyanine blue: A versatile and harmless stain for specimen observation. *Copeia,* 1997, 840–841.
https://doi.org/10.2307/1447302
Stamatakis, A. (2014) Stamatakis - 2014 - RAxML version 8 a tool for phylogenetic analysis and post-analysis of large phylogenies. 2010–2011.
Stein, D.L. (2012) Snailfishes (Family Liparidae) of the Ross Sea, Antarctica, and closely adjacent waters. *Zootaxa* 3285, 1–120.
Stein, D.L. (2016) Description of a new hadal *Notoliparis* from the Kermadec Trench, New Zealand, and redescription of *Notoliparis kermadecensis* (Nielsen) (Liparidae, Scorpaeniformes). *Copeia*, 104 (4), 907–920.
https://doi.org/10.1643/CI-16-451
Stein, D.L., Chernova, N. & Andriashev, A.P. (2001) Snailfishes (Pisces: Liparidae) of Australia, including descriptions of

thirty new species. *Records of the Australian Museum* 53, 341–406.
https://doi.org/10.3853/j.0067-1975.53.2001.1351
Steinke, D., Zemlak, T.S., Gavin, H. & Hebert, P.D.N. (2009) DNA barcoding fishes of the Canadian Pacific. *Marine Biology,* 156 (12), 2641–2647.
https://doi.org/10.1007/s00227-009-1284-0
Tamura, K. & Nei, M. (1993) Estimation of the number of nucleotide substitutions in the control region of mitochondrial DNA in humans and chimpanzees. *Molecular Biology and Evolution,* 10, 512–526.
Tamura, K., Stecher, G., Peterson, D., Filipski, A. & Kumar, S. (2013) MEGA6: Molecular Evolutionary Genetics Analysis version 6.0. *Molecular Biology and Evolution,* 30, 2725–2729.
https://doi.org/10.1093/molbev/mst197
Taylor, W.R. (1967a) *An enzyme method of clearing and staining small vertebrates*. Smithsonian Press, Washington, D.C.
Taylor, W.R. (1967b) Outline of a method of clearing and staining tissues with pancreatic enzymes and staining bones of small vertebrates. *Turtox News* 45.
Tyler, C.R. & Sumpter, J.P. (1996) Oocyte growth and development in teleosts. *Reviews in Fish Biology and Fisheries*, 6 (3), 287–318.
https://doi.org/10.1007/BF00122584
Ward, R.D., Zemlak, T.S., Innes, B.H., Last, P.R. & Hebert, P.D.N. (2005) DNA barcoding Australia's fish species. *Philosophical Transactions of the Royal Society B,* 360, 1847–1857.
https://doi.org/10.1098/rstb.2005.1716
Wickam, H. (2009) *ggplot2: elegant graphics for data analysis*.
Yancey, P., Gerringer, M., Drazen, J., Rowden, A. & Jamieson, A. (2014) Marine fish may be biochemically constrained from inhabiting the deepest ocean depths. *Proceedings of the National Academy of Sciences of the United States of America,* 111, 4461–5.
https://doi.org/10.1073/pnas.1322003111
Zhang, J.-B. & Hanner, R. (2011) DNA barcoding is a useful tool for the identification of marine fishes from Japan. *Biochemical Systematics and Ecology,* 39 (1), 31–42.
https://doi.org/10.1016/j.bse.2010.12.017